PRAMANA
—journal of
physics

Vol. 50, No. 6,
June 1998
pp. 501–514

The power and beauty of $(\gamma, 2e)$ experiments

VOLKER SCHMIDT
Fakultät für Physik, Universität Freiburg, D-79104 Freiburg, Germany

Abstract. The power and beauty of energy- and angle-resolved two-electron emission in the double photoionization of atoms is demonstrated, concentrating on the particular shapes of the angular correlation patterns of the triple differential cross section. The cases selected are direct double photoionization in helium and neon as well as sequential double photoionization in xenon, both for equal and unequal energies of the emitted electrons.

Keywords. $(\gamma, 2e)$; double photoionization; triple differential cross sections.

PACS No. 32.80

1. Introduction

In double photoionization one photon interacts with an atom leading to the emission of two electrons, $(\gamma, 2e)$. Contrary to the well established related $(e, 2e)$ experiments, energy- and angle-resolved $(\gamma, 2e)$ experiments became feasible only in the last few years [1–3], mainly for two reasons; for double photoionization the cross section is extremely low, and one needs monochromatized synchrotron radiation which is limited in its availability.

Selecting specific examples, the power and beauty of energy- and angle-resolved $(\gamma, 2e)$ experiments will be demonstrated. The power comes from the fact that such measurements provide (except for a spin analysis of the emitted electrons) complete information on photon-induced double ionization. This enables detailed studies of aspects as (i) the break-up of three particles which are subject to their mutual Coulomb interactions, (ii) parametrizations which completely describe the process, (iii) dependences of the observables on atomic structure, energies and directions of the emitted electrons under different light polarizations, and (iv) different mechanisms leading to double ionization: the direct process with the simultaneous emission of two photoelectrons, the two-step process with photoelectron and subsequent Auger electron emission, or the resonance-affected double photoionization which lies between these two limiting cases.

The beauty of the experiments lies in the stimulating interplay between state-of-the-art experiments and theoretical formulations, and in the attractive presentation of the results. Essential points in this context are the simplicity and the study of a cross section which is highly differential. The simplicity comes from the initial channel which consists of a ground-state atom and a single photon with known interaction operator. The cross section is a triple differential cross section (TDCS), being differential with respect to the solid angles $d\Omega_1$ and $d\Omega_2$ into which electron emission occurs and in the energy interval dE for the energies E_1 and E_2 of the electrons which are connected by energy conservation ($E_1 + E_2 = E_{\text{exc}}$, with the excess energy E_{exc} given by the photon energy $h\nu$ minus the

double ionization energy E_I^{++}). Both points ensure that the role of electron correlations and the influence of symmetry requirements on the electron-pair wave function in the continuum become directly visible in the observed results. A rather illustrative way to present these observations are TDCS ($\mathbf{k}_1, \mathbf{k}_2$) patterns. These describe the angular correlation between both electrons where the momentum $\mathbf{k}_1$ of one electron is preselected and kept fixed, and the angle-dependent intensity of the coincident other electron with momentum $\mathbf{k}_2$ is shown in a polar plot.

There exist many possibilities to study TDCS patterns experimentally [4]; a new and extremely powerful method is cold target recoil-ion momentum spectroscopy (COLTRIMS) with coincident detection of one of the electrons which allows the extraction of the full double photoionization kinematics [5]. In this review, however, examples are given for experiments in which the momenta $\mathbf{k}_1$ and $\mathbf{k}_2$ are measured directly by electron spectrometry. For example, in our set-up [6] two cylindrical mirror analysers (CMA) are mounted in the xy-plane perpendicular to the photon beam which propagates in z-direction ('perpendicular plane geometry'). One CMA (with a lens at its entrance) selects electrons of energy E_1 and momentum $\mathbf{k}_1$ and is positioned at a fixed direction with respect to the electric field vector of the incident light. The other spectrometer, a double-sector CMA which selects electrons of energy E_2 and momentum $\mathbf{k}_2$ can be rotated around the photon beam axis. The double-sector CMA makes it possible to simultaneously collect data at two distinct angles $\hat{k}_2$.

In the following basic aspects and general features of the TDCS patterns will be discussed for the fundamental process of double photoionization in helium, for direct double photoionization in neon, and for two-step double photoionization in xenon, distinguishing for the latter the two cases of unequal and equal electron energies.

2. Direct double photoionization in helium

TDCS studies of helium are unique, because direct double photoionization is not perturbed by other competing processes, and the final state consists of three bare charged particles. This makes helium the ideal test case for the theoretical treatment of the three-particle break-up Coulomb problem. As a result of many investigations it can be concluded that only approaches which properly take into account this electron correlation in the final continuum state are able to describe the observed TDCS patterns. For these cases one can note two observations [7]: First, if the shapes of TDCS patterns for equal electron energies are considered, good agreement between theoretical and experimental data is found, but discrepancies exist for unequal electron energies. Second, if absolute TDCS values are considered, larger differences are found in different theoretical treatments. The only reported experimental determination of absolute TDCS values at 20 eV excess energy appears to be too small by a factor of two and to be inconsistent with the observed integral cross section [6, 7]. (The theoretical result of the most elaborate and sophisticated calculation [8] is consistent with the observed integral cross section.) Out of the plethora of TDCS studies in helium one example for equal and unequal electron energies shall be selected for a more detailed discussion.

Two particular helium TDCS ($E_1 = E_2 = 10$ eV) patterns are shown in figure 1. These patterns refer to observation of the emitted electrons in the perpendicular plane geometry

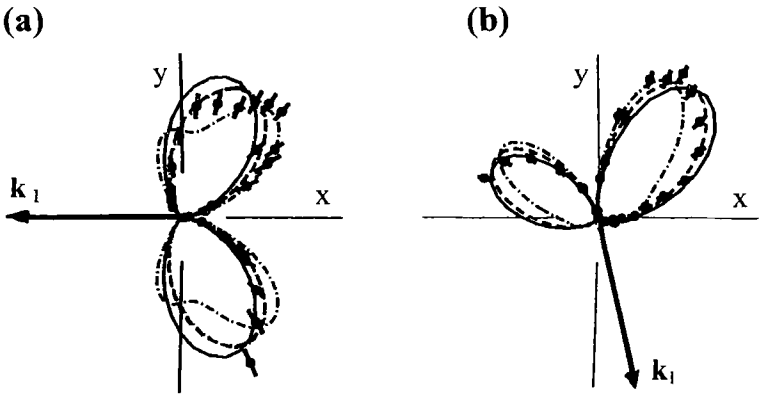

Figure 1. TDCS patterns for direct double photoionization in helium with $E_1 = E_2 = 10\,\text{eV}$. For details see text; experimental and theoretical data are from [9] and [8, 10–12], respectively; compare also [17].

and to photoionization by partially linearly polarized light ($S_1 = 0.55$; S_1 is the Stokes parameter which describes the relative excess of linear polarization along x-direction against linear polarization along y-direction; for details on the treatment of polarization in TDCS patterns see [13]). Good agreement can be noted between the experimental data (points with error bars) and several theoretical results scaled to the experimental values: the full curve (velocity form results of [10]) comes from a 3C calculation (the final-state wave function is approximated by a product of 3 Coulomb continuum wave function [14]), the broken curve (velocity form results of [8]) from a 2SC calculation (the final-state wave function is replaced by a product of two screened Coulomb functions [15] employing effective charges [16]), the dotted-dashed curve from a calculation of the wave packet propagation along the Wannier ridge [12].

Both the experimental and theoretical data in figure 1 reflect the following characteristic properties of the TDCS pattern: (i) Electron emission in opposite direction is prohibited. This is a purely quantum mechanical effect and arises from conditions imposed onto the electron pair wave function in the continuum with ${}^1P^0$ symmetry due to electron exchange ('unfavoured' character [18, 19]). This result is reflected also in the angular factor, see eq. (1) below, and in specific selection rules [10, 20]. (ii) Electron emission into the same direction is prohibited. This is a direct consequence of the correlated motion of the electrons and can be understood classically; electrons emitted with equal energies are prevented by their mutual Coulomb repulsion from traveling along the same trajectory. (iii) If one of the electrons is observed parallel to the major axis of the polarization ellipse (x-axis) of the incident light, the data in the upper half-plane are the mirror image of those in the lower half-plane (for completely linearly polarized light, $S_1 = 1$, rotational symmetry around the x-axis would exist).

In the context of helium TDCS ($E_1 = E_2 = E_{\text{exc}}/2$) patterns it is important to note that these patterns can be parametrized in a simple, yet exact form. Selecting the case of linearly polarized light one has [18]

$$\text{TDCS}(E_1 = E_2)_{\text{lin.pol.}x} = a(\cos\theta_1 + \cos\theta_2)^2 C(1,2). \tag{1}$$

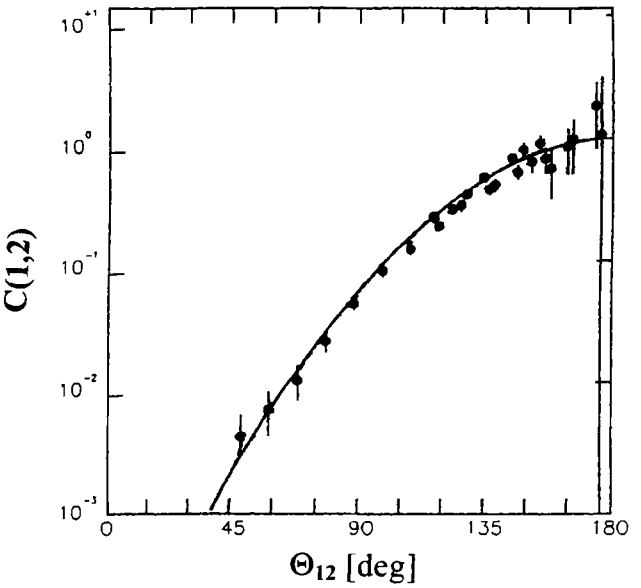

Figure 2. Correlation factor $C(1,2)$ for direct double photoionization in helium with $E_1 = E_2 = 10\,\text{eV}$, experimental values and Gaussian function with $\theta_{\text{fwhm}} = 91°$. For details see text, from [22].

a is a constant of proportionality and describes the strength of the process. $(\cos\theta_1 + \cos\theta_2)^2$ is an angular factor with θ_i being the angle of electron emission against the electric field vector (x-axis). For $\theta_2 = 180° - \theta_1$ and $\theta_1 = \theta_2 = 90°$ it leads to the two selection rules which prohibit electron emission in opposite directions and perpendicular to the electric field vector, respectively. $C(1,2)$ is the correlation factor (Sommerfeld factor) and reflects the Coulomb repulsion between the electrons. Its characteristic properties are $C(\mathbf{k}_1 = \mathbf{k}_2) = 0$ and $C(\mathbf{k}_1 = -\mathbf{k}_2) = 1$. Frequently this correlation factor is approximated by a Gaussian function in the relative angle θ_{12}, peaked at $\mathbf{k}_1 = -\mathbf{k}_2$, with a characteristic full-width-at-half-maximum value, θ_{fwhm}, and with $C(\mathbf{k}_1 = \mathbf{k}_2) =$ small (for the derivation see [21])

$$C(1,2) \approx \exp(-4\ln 2(180° - \theta_{12})^2/\theta_{\text{fwhm}}^2). \tag{2}$$

The quality of this approximation can be seen in figure 2 where experimental data (points with error bars) for the correlation factor of the TDCS patterns in figure 1 are in good agreement with the prediction from the Gaussian function of eq. (2), using $\theta_{\text{fwhm}} = 91°$. The value of this dynamical parameter is in agreement with theoretical predictions made within the extended Wannier ridge model [23]. With information on $C(1,2)$ and $(\cos\theta_1 + \cos\theta_2)^2$ it is now possible to plot for any angle settings, whether in the perpendicular plane geometry or not, the shapes of particular TDCS patterns (see examples in [4, 10, 17, 18]).

A typical TDCS pattern for high excess energy and unequal electron energies with a large E_1/E_2 ratio is shown in figure 3(a). In contrast to the characteristic features (i) and (ii) discussed in connection with figure 1, electron emission into opposite directions is

now possible (where it even leads to the intensity maximum) and as well electron emission into the same direction. These features can be understood, because at different electron energies the direct and exchange amplitudes of double photoionization do not cancel for $\mathbf{k}_1 = -\mathbf{k}_2$ and, thinking in a time-dependent picture for electron emission, the different electron velocities reduce the interaction time for Coulomb repulsion. Since the present example was obtained for completely linearly polarized light and the electron spectrometer at fixed direction is aligned with the electric field vector, the TDCS pattern has rotational symmetry around the x-axis. Within the experimental uncertainties and after adaption by an overall scaling factor the theoretical predictions from the 3C calculation (full curve, velocity form results [25]) and the 2SC calculation (broken curve, velocity form results [8]) are in good agreement with the experimental values. (For a treatment of unequal energies using wave packet propagation along the Wannier ridge see [26].)

It is also possible to describe a helium TDCS pattern with different electron energies by a simple and correct parametrization. For linearly polarized light one has [18]

$$\mathrm{TDCS}(E_1, E_2)_{\mathrm{lin.pol.}x} = |a_g(\cos\theta_1 + \cos\theta_2) + a_u(\cos\theta_1 - \cos\theta_2)|^2, \qquad (3)$$

where the energy- and θ_{12}-dependent amplitudes a_g and a_u reflect the symmetry properties against energy exchange, a_g is a gerade function, i.e., $a_g(E_1, E_2; \theta_{12}) = +a_g(E_2, E_1; \theta_{12})$, and a_u is an ungerade function, i.e., $a_u(E_1, E_2; \theta_{12}) = -a_u(E_2, E_1; \theta_{12})$. Hence, for equal energies a_u vanishes and eq. (3) reduces to eq. (1) with a_g^2 being the product of the constant a and the correlation factor $C(1,2)$. For unequal energies the nonvanshing portions of the real and imaginary part of a_u, together with the specific angular factor $(\cos\theta_1 - \cos\theta_2)$ then determine the TDCS shape. Equation (3) allows three particular observations to be

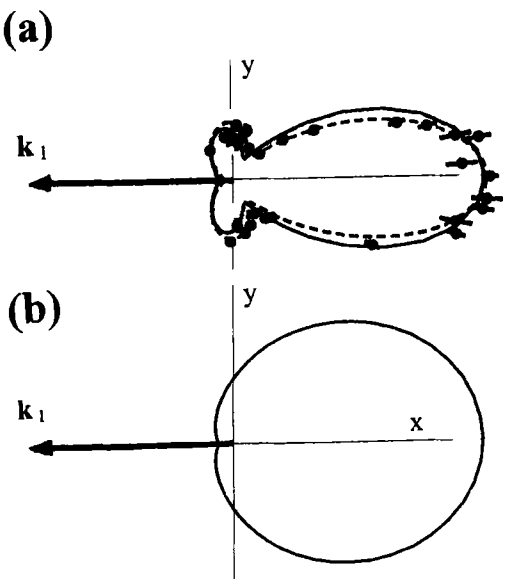

Figure 3. TDCS patterns for direct double photoionization in helium with $E_1 = 5\,\mathrm{eV}$, $E_2 = 47.9\,\mathrm{eV}$, part (a), and $E_1 = 47.9\,\mathrm{eV}$, $E_2 = 5\,\mathrm{eV}$, part (b). For details see text; experimental and theoretical data are from [24] and [8, 25], respectively.

made. First, there exist two complementary TDCS patterns with different shapes. They belong to interchanged energies of the electrons 1 and 2 (1 is the electron detected in the fixed spectrometer, 2 is the electron detected in the variable spectrometer). Both patterns are related to each other by simply changing in eq. (3) the sign of a_u. For the example in figure 3(a) the complementary TDCS pattern is shown in part (b) of this figure. Second, a continuous change in the E_1/E_2 ratio can lead to rather different shapes of the TDCS patterns (see figure 3); the intermediate case with $E_1 = E_2 = E_{exc}/2$ looks rather similar to the pattern in figure 1(a). Therefore, the evolution of such patterns by changing the E_1/E_2 ratio can provide a critical test for the quality of different theoretical approaches (see [7]). Third, Wannier theory predicts that for excess energies approaching zero the a_g amplitude will dominate the a_u amplitude and a_g becomes insensitive to the E_1/E_2 ratio [19, 27, 28]. Therefore, differences in the complementary patterns vanish and they look similar to TDCS ($E_1 = E_2 = E_{exc}/2$) patterns. Experimental confirmation has been given for excess energies of 4.0 eV [28] and 0.6 eV [29], as well as by the interpretation of COLTRIMS data at 1 eV [5, 17].

3. Direct double photoionization in neon

For double photoionization in helium the dipole selection rules require the electron-pair wave function in the continuum to couple to a final $^1P^0$ state. For rare gas atoms heavier than helium, the remaining np^4 electrons in the final ionic state can couple to form $^1S^e$, $^3P^e$ and $^1D^e$ states, so that different LSJ-coupled continuum channels are possible. (For a study on $3s3p^5\,^1P^0, ^3P^0$ final ionic states in argon see [30].) Since, within LSJ-coupling, the complete final state must be $^1P^0$, the LSΠ-terms of the continuum function are $^1P^0$ for the $np^4\,^1S^e$ ion, $^3P^0$ and $^3D^0$ for the $np^4\,^3P^e$ ion, and $^1P^0$, $^1D^0$ and $^1F^0$ for the $np^4\,^1D^e$ ion. There is particular interest associated with each of these cases: For $2p^4\,^1S^e$ the continuum function is $^1P^0$, as in helium, but because of different orbital angular momenta in the initial states, $l_i = 0$ for helium and $l_i = 1$ for neon, the composition of the electron-pair wave-function in the continuum can differ. For $np^4\,^3P^e$ the contributing continuum function $^3P^0$ is exceptional, because it has different symmetry properties ('favoured' character [18, 19]) which are connected with different angular functions and/or selection rules. In addition, the $^3P^0$ and $^3D^0$ continuum channels interfere. For $np^4\,^1D^e$ interference effects between three continuum channels exist, but their influence might be masked by the general conditions set to these continuum channels by the 'unfavoured' symmetry properties which result in a similarity of the individual amplitudes. Because of these properties it is therefore necessary to conduct a state-dependent study of double photoionization.

Before turning to state-dependent TDCS patterns for direct double photoionization in neon leading to $np^4\,^1S^e, ^3P^e, ^1D^e$, the important point of possible competing processes which proceed via an intermediate state to the same doubly charged ionic states must be addressed. In the present example the strongest disturbance by such processes comes from $2s2p^5nl$ photosatellites with a $\mathbf{k}_p$ photoelectron and the autoionization decay of these satellites to $2s^22p^4\,^1S^e, ^3P^e, ^1D^e$ where the electron $\mathbf{k}_a$ is emitted. In principle this sequential or indirect process will interfere with direct double photoionization having the same symmetry (resonance affected double photoionization [31]). As a result of such sequential processes the smooth energy distribution of the double ionization continuum of

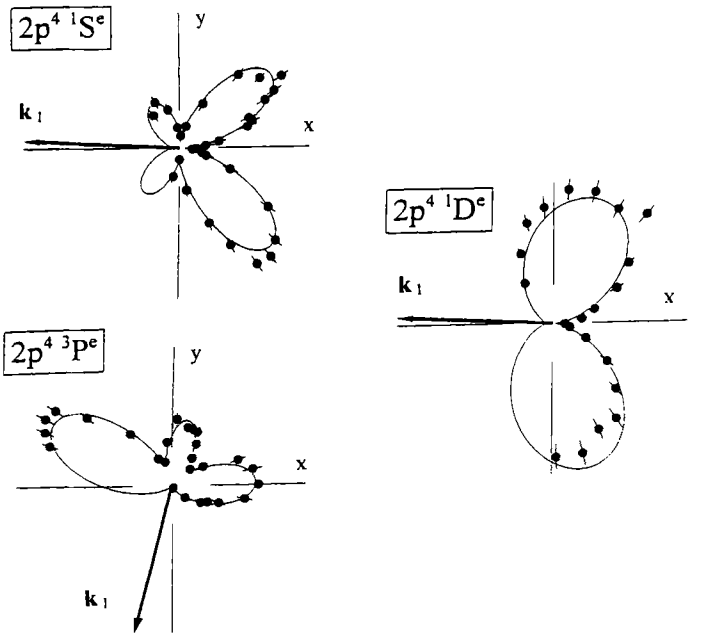

Figure 4. State-dependent TDCS patterns for direct double photoionization in the $2p^6$ shell of neon with equal sharing of the excess energy. For details see text; from [34].

direct processes gets a rich structure of discrete photoelectron and autoionization electron lines [32, 33]. Hence, in order to study direct double photoionization, these discrete processes have to be clearly identified and then avoided by properly selecting the energies E_1 and E_2 (see demonstration in [31]).

A collection of $np^4\ {}^1S^e, {}^3P^e, {}^1D^e$ state-dependent TDCS patterns for direct double photoionization in neon is shown in figure 4. The data refer to equal energy sharing of the respective excess energies and to observation in the perpendicular plane geometry; the solid curve is a fit to the experimental values (points with error bars) based on a simple model to parametrize these TDCS patterns which will be partly discussed below. Comparing the TDCS $(2p^4\ {}^1S^e)$ pattern with that of helium, figure 1(a), one notes the same characteristic features (i) to (iii) discussed in connection with figure 1. However, two additional lobes appear in the neon case. The origin of these lobes can be traced back to an interference effect between $[\epsilon l\, \epsilon l'\ {}^1P^0]$ and $[\epsilon l\, \epsilon(l'+1)\ {}^1P^0]$ channels in the electron-pair wave function in the continuum [35]. The existence of such channels follows from a simple parametrization of this TDCS based on uncorrelated wave functions for the initial and final states (responsible for $2p \rightarrow \epsilon s$ and $2p \rightarrow \epsilon d$ photoionization channels), in which core relaxation is included (responsible for $2p \rightarrow \epsilon p$ shake-off) and electron–electron Coulomb repulsion is taken into account by a correlation factor $C(1,2)$. It leads to [34, 35]

$$\mathrm{TDCS}(E_1 = E_2)_{\mathrm{lin.pol}.x} = \left| D_{ps} + \frac{\mathrm{e}^{i\Delta_{ds}}}{\sqrt{2}} (3\cos\theta_{12} - 1) D_{pd} \right|^2 \times (\cos\theta_1 + \cos\theta_2)^2 C(1,2), \tag{4}$$

where in the uncorrelated limit Δ_{ds} is the phase difference between the ϵd and ϵs partial waves, and the radial matrix elements D_{ps} and D_{pd} are products of the dipole photoionization and monopole shake-off integrals. Comparing this parametrization with the one of eq. (1) it becomes evident that the initial state orbital is responsible for the difference between neon and helium; within the same model, the first factor in eq. (4) has to be replaced for the helium case by only one radial matrix element, D_{sp}, which corresponds to the $1s \rightarrow \epsilon p$ dipole and the $1s \rightarrow \epsilon s$ monopole transition. (For more details see [13, 34]; for critical comments on the model parametrization see [36]; for theoretical results which reproduce the characteristic features of these experimental data see [37] for a wave packet propagation along the Wannier ridge, and [38] for a 3C continuum function calculation; for first evidence of such an initial orbital effect see [39].)

As expected, the TDCS ($2p^4\,{}^3P^e$) pattern in figure 4 differs remarkably from the patterns discussed so far: due to the 'favoured' symmetry of the ${}^3P^0$ continuum function electron emission is possible now into opposite directions (except for the case that $\mathbf{k}_1$ is parallel to the electric field vector of linearly polarized light [19, 20]). For this back-to-back emission the TDCS intensity is entirely due to the ${}^3P^0$ contribution, in the other lobes the intensity comes, within the given model, from constructive interference of ${}^3P^0$ and ${}^3D^0$. (For results of a 3C calculation see [38]; compare also the related case of $4p^4\,{}^3P^e$ double photoionization in krypton with experimental data [1] and theoretical results from the wave packet propagation along the Wannier ridge [40]). Finally, the neon TDCS ($2p^4\,{}^1D^e$) pattern in figure 4 shows a simple double-lobe structure rather similar to helium, in agreement with the expected dominance of 'unfavoured' characteristics in the interfering continuum channels (compare 3C results in [38]).

4. Two-step double ionization in xenon for $E_p \neq E_A$

As example of a 2-step double photoionization process $4d_{5/2}$ photoionization in xenon with subsequent N_5–$O_{2,3}O_{2,3}\,{}^1S_0$ Auger decay shall be selected. In this case the process proceeds via a well-defined intermediate state with inherent level width Γ and all conditions for the application of the traditional 2-step formulation are fulfilled, provided the kinetic energies of both emitted electrons are different and, if present, effects of post-collision interaction (PCI) are properly taken into account [41]. As a consequence, the properties of the first step, photoionization, decouple from those of the second step, Auger decay. The only link between the two is in the form of an angle-dependent alignment tensor [42]. There is no continuous energy distribution as in direct double photoionization, but two electrons appear with a Lorentzian distribution (full-width-at-half-maximum value Γ) at the nominal kinetic energies $E_p^0 = h\nu - E_I^+$ and $E_A^0 = E_I^+ - E_I^{++}$, and these electrons are identified with the photoelectron and the Auger electron, respectively (E_I^+ and E_I^{++} are the energies for $4d_{5/2}^{-1}$ single and $5p^{-2}\,{}^1S$ double ionization). Furthermore, the electron-pair wave function in the continuum factorizes into that of the photoelectron and the Auger electron. In the example given one has the photoionization channels $4d_{5/2}^{-1}\epsilon f_{7/2} J = 1, 4d_{5/2}^{-1}\epsilon f_{5/2} J = 1, 4d_{5/2}^{-1}\epsilon p_{3/2} J = 1$ with attached dipole matrix elements D_+, D_0, D_-, respectively, and the partial wave $\epsilon d_{5/2}$ for the selected Auger transition. Such a finite number of channels involved makes it possible to derive an explicit parametrization of the TDCS into factors which depend on the photoionization matrix

elements and the direction $\hat{k}_p$ of photoelectron emission and factors which depend on the Auger decay matrix elements and the direction $\hat{k}_A$ of Auger electron emission [42]. Because in the selected example only one partial wave of the Auger electron is possible, the second factor reduces to known numerical values, except for an overall intensity value which is not relevant for the shape of TDCS patterns. Therefore, relative TDCS patterns for the selected 2-step double ionization process depend in a known way on the emission angles $\hat{k}_p$ and $\hat{k}_A$, and on the photoionization matrix elements D_+, D_0, D_-. This characteristic of a TDCS pattern adds information to the initial photoionization process and, in conjunction with other observables (partial photoionization cross section, angular distribution of non-coincident photoelectrons and non-coincident Auger electrons), it can be used to extract photoionization matrix elements, including their relative phases ('complete experiments', see [2, 43, 44]).

Two examples of TDCS patterns of $4d_{5/2}$ photoionization in xenon with subsequent N_5–$O_{2,3}O_{2,3}$ $^1S_0$ Auger decay are shown in figure 5. The data are for completely linearly polarized light (field vector along x) and for observation in the perpendicular plane geometry. In (a) the photoelectron is observed at a fixed direction and the Auger electron spectrometer is turned around, in (b) the complementary case is shown. For these patterns one can note the following properties: (i) Because one of the electrons is observed in a direction parallel to the electric field vector of the incident light, both patterns have rotational symmetry around the x-direction. (ii) Pattern (b) has more structure than pattern (a). This can be traced back to the connection of orbital angular momenta with spherical harmonics. Using for reasons of simplicity only an ϵf partial wave for the photoelectron and an ϵd partial wave for the Auger electron, the essential part in the angular correlation function is given by $Y_{3m}(\hat{k}_p)Y_{2-m}(\hat{k}_A)$ terms which lead for fixed photoelectron direction to TDCS $\propto |Y_{20}(\hat{k}_A)|^2$, and for fixed Auger electron direction to TDCS $\propto |Y_{30}(\hat{k}_p)|^2$ (compare in this context figure 6(a) and [45]). (iii) Both patterns are

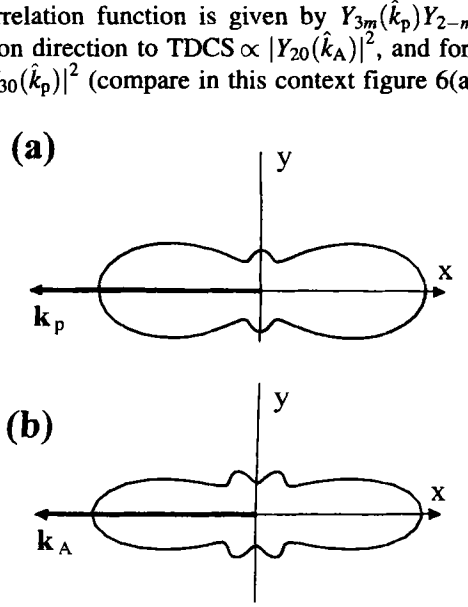

Figure 5. TDCS patterns for 2-step double photoionization in xenon, $4d_{5/2}$ photoionization and subsequent $N_5 - O_{2,3}O_{2,3}$ $^1S_0$ Auger decay at 94.5 eV photon energy, $E_p = 26.95$ eV, $E_A = 29.97$ eV. (**a**) Photoelectron detection at fixed position, $\mathbf{k}_p$; (**b**) Auger electron detection at fixed position, $\mathbf{k}_A$. For details see text; from [43].

symmetric against reflection on the yz-plane. This property is in strong contrast to TDCS patterns of direct double photoionization. It has its origin in the different energies of the emitted electrons and in the time delay between the emission of the photoelectron and the subsequent Auger electron.

The TDCS patterns discussed so far for direct and 2-step double photoionization all refer to completely (or partially) linearly polarized light. If circularly polarized light is used, the patterns can have remarkably different shapes for right- and left-circular polarization. This phenomenon is called circular dichroism in the angular distribution patterns [46–48]. The condition for the observation of circular dichroism can be inferred easily from the following three-finger rules: First, the electron momenta $\mathbf{k}_1$ and $\mathbf{k}_2$ and the spin projection of the photon along its propagation direction (helicity presentation for right and left circularly polarized light) are identified with three fingers. Second, a change of circular polarization is identical to a change of the fingers from one hand to the same fingers of the other hand. Third, non-vanishing circular dichroism occurs if the fingers set on the right hand do not coincide with the fingers set on the left hand. As particular result of these rules one obtains for the present case of interest that circular dichroism is possible in the perpendicular plane geometry, but there it vanishes for equal energies of the electrons (the two fingers for $\mathbf{k}_1$ and $\mathbf{k}_2$ become indistinguishable). For the first experimental observations of circular dichroism in TDCS patterns of 2-step double ionization see [49] and for direct double photoionization see [50].

5. Sequential double ionization in xenon for $E_p \approx E_A$

Dramatic changes in the TDCS patterns of a 2-step double ionization process are expected if the restriction of different energies of the photoelectron and the Auger electron is relinquished: In the case of $E_p \approx E_A$ the traditional 2-step formula fails and must be replaced by a formulation which treats the process as a resonance embedded in the double ionization continuum [51]. Application of this theory then leads for the case of $4d_{5/2}$ photoionization with subsequent N_5–$O_{2,3}O_{2,3}$ $^1S_0$ Auger decay to the following result ([52]), for a detailed treatment of the present example see also [53, 54])

$$\begin{aligned}
&\mathrm{TDCS}(\mathbf{k}_1, \mathbf{k}_2)_{\mathrm{lin.pol}.x} \\
&= \frac{1}{2}\left| \sum_M \left(\frac{\langle \mathrm{Xe}^{++}\mathbf{k}_1 | H_{\mathrm{el}} | \mathrm{Xe}^+(M)\rangle \langle \mathrm{Xe}^+(M)\mathbf{k}_2 | H_{\mathrm{int}} | \mathrm{Xe}\rangle}{E_1 - E_A^0 + i\Gamma/2} \right.\right. \\
&\quad \left.\left. + (-1)^S \frac{\langle \mathrm{Xe}^{++}\mathbf{k}_2 | H_{\mathrm{el}} | \mathrm{Xe}^+(M)\rangle \langle \mathrm{Xe}^+(M)\mathbf{k}_1 | H_{\mathrm{int}} | \mathrm{Xe}\rangle}{E_2 - E_A^0 + i\Gamma/2} \right) \right|^2 . \qquad (5)
\end{aligned}$$

The expression states that, due to electron exchange, two amplitudes occur which are combined with 'plus' and 'minus' signs, corresponding to the values of the total spin $S = 0$ or $S = 1$ of the electron-pair wave function, respectively. Each amplitude consists of a photoionization matrix element (transition operator H_{int}) and an Auger transition matrix element (operator H_{el}), and in these the role of the electron momenta $\mathbf{k}_1$ and $\mathbf{k}_2$ is interchanged. The importance of each amplitude is governed by the energy denominator: For very different energies E_1 and E_2 the first denominator resonates for $E_1 = E_A^0$ (energy conservation implies $E_2 = E_p^0$) and there the second denominator is negligible, i.e., the

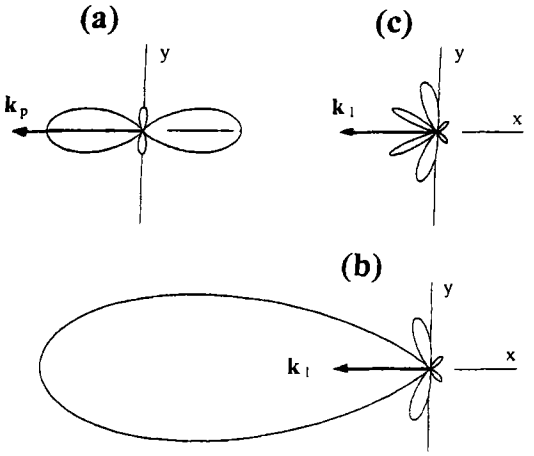

Figure 6. TDCS patterns for sequential double photoionization in xenon, $4d_{5/2}$ photoionization and subsequent $N_5 - O_{2,3}O_{2,3}\ ^1S_0$ Auger decay, at photon energies to demonstrate (**a**) the off-the-resonance case with $E_p = 24.97\,\text{eV}$, $E_A = 29.97\,\text{eV}$; (**b**) the on-the-resonance case with $E_1 = E_2 = 29.97\,\text{eV}$, omitting PCI effects; (**c**) the on-the-resonance case with $E_1 = E_2 = 29.97\,\text{eV}$, including PCI effects. For details see text; from [57].

electron momenta $\mathbf{k}_1$ and $\mathbf{k}_2$ can be identified with $\mathbf{k}_A$ and $\mathbf{k}_p$. Similarly, the second denominator dominates for the complementary case with $\mathbf{k}_1 = \mathbf{k}_p$ and $\mathbf{k}_2 = \mathbf{k}_A$. Hence, one is lead back to the complementary TDCS patterns shown in figure 5. However, for $E_1 \approx E_2$ both amplitudes are of equal importance and interference effects occur [52]. In this context two points must be emphasized. First, these interference effects are a one-channel phenomenon (no other competing pathways exist to photoionization with subsequent Auger decay). This makes these interferences fundamentally different from cases where indistinguishable pathways exist which lead to a common final state [55, 56]. Second, the interference is important only in the energy range of Γ and has largest effect for $E_p^0 = E_A^0$ ('on the resonance').

In order to demonstrate the interference effects in the sequential process of $4d_{5/2}$ photoionization in xenon with subsequent N_5–$O_{2,3}O_{2,3}\ ^1S_0$ Auger decay, some TDCS patterns are shown in figure 6. They refer to linearly polarized incident light (field vector along x) and observation in the perpendicular plane geometry, and they have been calculated under the simplifying approximation that spin-orbit effects can be neglected, as well as the ϵp partial wave of the photoelectron against its ϵf partial wave. For comparison, the off-the-resonance case is shown in part (a) (compare with figure 5(a), but note that all photoionization amplitudes are taken into account), the on-the-resonance case is plotted in parts (b) and (c). The on-the-resonance case in parts (b) and (c) clearly demonstrates the destructive interference which gives zero intensity at $\mathbf{k}_2 = -\mathbf{k}_1$, and in part (b) the constructive interference occuring at the opposite directions. The origin of this interference can be traced back to the $^1P^0$ symmetry of the electron-pair wave function in the continuum, i.e., to the same origin as shown for direct double photoionization in helium with $E_1 = E_2$. For experimental verifications of this destructive interference effect see [53, 58, 59] and [60].

Concentrating in figure 6(b) on the angular region with constructive interference one must extend the discussion, because also in a sequential process Coulomb interactions between the charged particles play a role and must be taken into account. Such interactions are referred to in the literature as post-collision interaction (PCI) [61]. As a result of angle-dependent PCI the actual energies of the emitted electrons are modified: For small relative angles θ_{12} the Auger electron loses energy and the photoelectron gains the same amount ([62, 63, 64]; note that these energy shifts are opposite to those observed in the non-coincident case in the near threshold region). If such angle-dependent PCI effects are implemented into the amplitudes of eq. (5) one gets the TDCS pattern in figure 6(c). Remarkably, this pattern has the same characteristic features (i) to (iii) as discussed in connection with figure 1(a) for direct double photoionization in helium at equal energies. This means, for $E_1 = E_2$ differences in direct and sequential double photoionization disappear.

Comparing in figure 6 parts (b) and (c), the question arises into which channels the huge intensity from the constructive portions of the TDCS pattern (b) is transferred. The analysis shows that PCI shifts intensity to other energies. These energy transfers are also important for the off-the-resonance case with $E_p^0 \leq E_A^0$. There it can happen that formerly well separated coincident energy distributions located around the nominal values $E_1 = E_p^0$ with $E_2 = E_A^0$ or $E_2 = E_p^0$ with $E_1 = E_A^0$ are modified so strongly by PCI that the two amplitudes in eq. (5) with implemented PCI effects gain weight and lead to PCI induced interferences in the resulting energy distributions [54].

6. Conclusion

For specific examples it has been demonstrated that the shape of TDCS patterns provides detailed information on the underlaying process of double photoionization and, analysing the TDCS shapes in terms of appropriate parameterizations, on the angle-dependences and the dynamical parameters. For the fundamental three-body system helium a great deal of understanding has been achieved already. Studies in other elements are just at the beginning. However, for the few cases touched slightly in this report interesting new features could be demonstrated. Of particular interest are differences and similarities in double photoionization described as a direct or sequential process. It can be expected that forthcoming studies in this direction will widely open our understanding of two electrons emitted from different systems and/or by different mechanisms into the continuum.

Acknowledgements

The author thanks all members of his research group for their contributions and stimulating discussions, and the Deutsche Forschungsgemeinschaft for financial support in the SFB 276, TP B5.

References

[1] J Mazeau, P Selles, D Waymel and A Huetz, *Phys. Rev. Lett.* **67**, 820 (1991)
[2] B Kämmerling and V Schmidt, *Phys. Rev. Lett.* **67**, 1848 (1991); *Phys. Rev. Lett.* **69**, 1145 (1992)
[3] O Schwarzkopf, B Krässig, J Elmiger and V Schmidt, *Phys. Rev. Lett.* **70**, 3008 (1993)

[4] V Schmidt, in *Atomic and Molecular Photoionization*, Proc. of Oji Intern. Seminar, Tsukuba/Japan, edited by A Yagishita and T Sasaki (Universal Academy Press, Tokyo/Japan, 1996) p. 21–30
[5] R Dörner, J M Feagin, C L Cocke, H Bräuning, O Jagutzki, M Jung, E P Kanter, H Khemliche, S Kravis, V Mergel, M H Prior, H Schmidt-Böcking, J Ullrich, M Unverzagt and T Vogt, *Phys. Rev. Lett.* **77**, 1024 (1996)
[6] O Schwarzkopf and V Schmidt, *J. Phys.* **B28**, 2847 (1995); *J. Phys.* **B29**, 1877 (1996)
[7] M Pont, R Shakeshaft, F Maulbetsch and J S Briggs, *Phys. Rev.* **A53**, 3671 (1996)
[8] M Pont and R Shakeshaft, *Phys. Rev.* **A51**, R2676 (1995)
[9] O Schwarzkopf, PhD Thesis *Experimentelle Untersuchungen zur Doppel photoionisation von xenon und helium*, University Freiburg, unpublished (1995); see also [3, 6]
O Schwarzkopf, B Krässig and V Schmidt, *J. Phys. IV Colloq. C6 Suppl. J. Phys. II*, **3**, 169 (1993)
[10] F Maulbetsch and J S Briggs, *J. Phys.* **B26**, L647 and 1679 (1993)
[11] F Maulbetsch, M Pont, J S Briggs and R Shakeshaft, *J. Phys.* **B28**, L341 (1995)
[12] A K Kazansky and V N Ostrovsky, *J. Phys.* **B28**, 1453 (1995)
[13] S J Schaphorst, B Krässig, O Schwarzkopf, N Scherer, V Schmidt, P Lablanquie, L Andric, J Mazeau and A Huetz, *J. Electron Spectrom. Relat. Phenom.* **76**, 229 (1995)
[14] P J Redmond (1973) unpublished, presented without derivation by L Rosenberg in *Phys. Rev.* **D8**, 1833 (1973)
S P Merkuriev, *Theor. Math. Phys.* **32**, 680 (1977)
C Garibotti and J E Miraglia, *Phys. Rev.* **A21**, 572 (1980)
M Brauner, J S Briggs and H Klar, *J. Phys.* **B22**, 2265 (1989)
[15] M R H Rudge and M J Seaton, *Proc. R. Soc. London Ser.* **A283**, 262 (1996)
[16] M R H Rudge, *Rev. Mod. Phys.* **40**, 564 (1958)
C Pan and A F Starace, *Phys. Rev. Lett.* **67**, 185 (1991)
S Jetzke and F H M Faisal, *J. Phys.* **B25**, 1543 (1992)
[17] J M Feagin, *J. Phys.* **B29**, L551 (1996)
[18] A Huetz, P Selles, D Waymel and J Mazeau, *J. Phys.* **B24**, 1917 (1991)
[19] C H Greene and A R P Rau, *Phys. Rev. Lett.* **48**, 533 (1982): *J. Phys.* **B16**, 99 (1983)
A D Stauffer, *Phys. Lett.* **91a**, 114 (1982)
[20] F Maulbetsch and J S Briggs, *J. Phys.* **B28**, 551 (1995)
[21] M Brauner, J S Briggs and H Klar, *J. Phys.* **B22**, 2265 (1989)
[22] O Schwarzkopf, PhD Thesis *Experimentelle Untersuchungen zur Doppel photoionisation von xenon und helium*, University Freiburg, unpublished (1995)
[23] A K Kazansky and V N Ostrovsky, *J. Phys.* **B26**, 2231, (1993)
[24] O Schwarzkopf, B Krässig, V Schmidt, F Maulbetsch and J S Briggs, *J. Phys.* **B27**, L347 (1994)
[25] F Maulbetsch and J S Briggs, *J. Phys.* **B27**, 4095 (1994)
[26] A K Kazansky and V N Ostrovsky, *Phys. Rev.* **A51**, 3698 (1995)
[27] R Peterkop, *J. Phys.* **B16**, L587 (1983)
[28] P Lablanquie, J Mazeau, L Andric, P Selles and A Huetz, *Phys. Rev. Lett.* **74**, 2192 (1995)
[29] G Dawber, L Avaldi, A G McConkey, H Rojas, M A MacDonald and G C King, *J. Phys.* **B28**, L271 (1995)
[30] J Mazeau, P Lablanquie, P Selles, L Malegat and A Huetz, *J. Phys.* **B30**, L293 (1997)
[31] B Krässig, O Schwarzkopf and V Schmidt, *J. Phys.* **B26**, 2589 (1993)
[32] U Becker, R Wehlitz, O Hemmers, B Langer and A Menzel, *Phys. Rev. Lett.* **63**, 1054 (1989)
[33] M Pahler, C D Caldwell, S J Schaphorst and M O Krause, *J. Phys.* **B26**, 1617 (1993)
[34] B Krässig, S J Schaphorst, O Schwarzkopf, N Scherer and V Schmidt, *J. Phys.* **B29**, 4255 (1996)
[35] S J Schaphorst, B Krässig, O Schwarzkopf, N Scherer and V Schmidt, *J. Phys.* **B28**, L233 (1995)
[36] L Malegat, P Selles and A Huetz, *J. Phys.* **B30**, 251 (1997)
L Malegat, P Selles, P Lablanquie, J Mazeau and A Huetz, *J. Phys.* **B30**, 263 (1997)
[37] A K Kazansky and V N Ostrovsky, *Phys Rev.* **A52**, 1775 (1995)

[38] A W Malcherek, F Maulbetsch and J S Briggs, *J Phys.* **B26**, 4127 (1996)
[39] D Waymel, L Andric, J Mazeau, P Selles and A Huetz, *J. Phys.* **B26**, L123 (1993)
[40] A K Kazansky and V N Ostrovsky, *J. Phys.* **B28**, L333 (1995)
[41] V Schmidt, *Rep. Prog. Phys.* **55**, 1483 (1992)
[42] N M Kabachnik, *J. Phys.* **B25**, L389 (1992)
[43] B Kämmerling and V Schmidt, *J. Phys.* **B26**, 1141 (1993)
[44] S J Schaphorst, Q Qian, B Krässig, P van Kampen, N Scherer and V Schmidt, *J. Phys.* **B30**, 4003 (1997)
[45] L Végh and R L Becker, *Phys. Rev.* **A46**, 2445 (1992)
[46] J Berakdar and H Klar, *Phys. Rev. Lett.* **69**, 1175 (1992)
J Berakdar, H Klar, A Huetz and P Selles, *J. Phys.* **B26**, 1463 (1993)
[47] N M Kabachnik and V Schmidt, *J. Phys.* **B28**, 233 (1995)
[48] S Heinäsmäki and T Åberg, *17th Int. Conf. on X-Ray and Inner-Shell Processes* (Hamburg, Germany) (Abstracts) contributed paper TuPo66 (1996)
[49] K Soejima, M Shimbo, A Danjo, K Okuno, E Shigemasa and A Yagishita, *J. Phys.* **B29**, L367 (1996)
[50] J Viefhaus, L Avaldi, G Snell, M Wiedenhöft, R Hentges, A Rüdel, F Schäfers, D Menke, U Heinzmann, A Engelns, J Berakdar, H Klar and U Becker, *Phys. Rev. Lett.* **77**, 3975 (1996)
[51] T Åberg, *Phys. Scr.* **21**, 495 (1980)
T Åberg and G Howat, Theory of the Auger effect, *Corpuscles and Radiation in Matter, Encyclopedia of Physics* edited by W Mehlhorn (Springer Berlin, 1982) vol. 31, p. 469
J Tulkki, G B Armen, T Åberg, B Crasemann and M H Chen, *Z. Phys.* **D5**, 241 (1987)
[52] L Végh, R Becker and J H Macek, *15th Int. Conf. on X-Ray and Inner-Shell Processes* (Knoxville, TN) (Abstracts) contributed paper D11 (1990)
L Végh and J H Macek, *Phys. Rev.* **A50**, 4031 (1994)
[53] O Schwarzkopf and V Schmidt, *J. Phys.* **B29**, 3023 (1996)
[54] S A Sheinerman and V Schmidt, *J. Phys.* **B30**, 1677 (1997)
[55] J P van den Brink, J van Eck and H G M Heideman, *Phys. Rev. Lett.* **61**, 2106 (1988)
J A de Gouw, J van Eck, A C Peters, J van der Weg and H G M Heideman, *Phys. Rev. Lett.* **71**, 2875 (1993)
[56] L Végh, *Phys. Rev.* **A50**, 4036 (1994)
[57] V Schmidt, O Schwarzkopf and S J Schaphorst, *5th Int. Workshop: Autoionization Phenomena in Atoms (Dubna, Russia)* (Invited Talks) edited by V V Balashov, A N Grum-Grzhimailo and E A Romanovsky (Moscow University Press, 1996), p. 20
[58] S J Schaphorst, A Jean, O Schwarzkopf, P Lablanquie, L Andric, A Huetz, J Mazeau and V Schmidt, *J. Phys.* **B29**, 1901 (1996)
[59] U Becker, private communication (1996)
[60] J P Doering, M A Coplan, J W Cooper and J H Moore, *Phys. Rev.* **A41**, 535 (1990)
[61] M Yu Kuchiev and S A Sheinerman, *Sov. Phys. Usp.* **32**, 569 (1989)
[62] M Yu Kuchiev and S A Sheinerman, *Sov. Phys. JETP* **63**, 986 (1986); *J. Phys.* **B21**, 2027 (1988)
[63] P van der Straten, R Morgenstern and A Niehaus, *Z. Phys.* **D8**, 35 (1988)
[64] G B Armen, *Phys. Rev.* **A37**, 995 (1988)